Stochastic Properties of Turbulence Excited Rotor Blade Vibrations

GOPAL H. GAONKAR* AND KURT H. HOHENEMSER†
Washington University, St. Louis, Mo.

The developed analytical methods are applicable to the linearized equations of blade motion up to high rotor advance ratios. Rigid flapping blades with elastic flapping restraint are stipulated, only vertical turbulence components are considered and the ratio of turbulence scale length over rotor radius L/R is assumed to be large. On the basis of computed threshold crossing expectations, the blade response can be described as a quasi-coherent narrow-band random process. The limiting case of infinite L/R is easy to compute and to interpret and yields conservative values for the mean square blade response. Numerical analysis for a slowed unloaded rotor based on low-altitude turbulence data indicates in the absence of gust alleviating device an appreciable probability of excessive blade flapping or flap-bending.

Nomenclature

w	= vertical turbulence velocity, ft
L	= turbulence scale length, ft
r	= longitudinal space coordinate, ft
ω_r	= spacewise circular frequency, rad/ft
σ	= standard deviation
ω	= timewise circular frequency, rad/sec.
$\bar{\omega}$	= ω/Ω = nondimensional frequency
f	= $\omega/2\pi$ = timewise frequency, 1/sec
Ω	= angular rotor speed, rad/sec
t,τ	= time, sec. (τ used in autocorrelation function)
$\bar{t}$	= Ωt, $\bar{\tau} = \Omega\tau$ = nondimensional time
V	= flight velocity, fps
R	= rotor radius, ft
$\phi,(S)$	= one-sided (two-sided) power spectral density
$R_{\text{subscripts}}$	= autocorrelation function
μ	= rotor advance ratio
λ	= $w/\Omega R$ = nondimensional vertical turbulence velocity
Λ	= Fourier transform of λ
a	= $2\mu/(L/R)$ = turbulence parameter
B	= blade tip loss factor
β	= flapping angle
γ	= Lock blade inertia number
$C(\bar{t})$	= aerodynamic blade damping
$K(\bar{t})$	= aerodynamic blade stiffness
$B(\bar{t})$	= aerodynamic input modulation
ω_β	= natural flapping frequency at $\Omega = 0$
P^2	= $1 + \omega_\beta^2/\Omega^2$ = elastic flapping restraint parameter
$r(\bar{t})$	= cross correlation coefficient
$y_c(\omega,\bar{t})$	= response to input $0.5\gamma B(\bar{t})\cos(\omega t)$
$y_s(\omega,\bar{t})$	= response to input $0.5\gamma B(\bar{t})\sin(\omega t)$
$E[N_+(\zeta,\bar{t})]$	= expected number per unit time of positive crossings of level ζ
$E[M_+(\zeta)]$	= expected number per rotor revolution of positive crossings of level ζ
$Re(\eta)$	= stability parameter in Floquet solution

Subscript

*	= conjugate complex

Presented as Paper 70-548 at the AIAA Atmospheric Flight Mechanics Conference, Tullahoma, Tennessee, May 13–15, 1970; submitted May 28, 1970; revision received October 19, 1970. Sponsored by the Ames Directorate, U. S. Army Air Mobility R & D Lab. 1 under Contract NAS2-4151.

* Research Affiliate Professor, Deptartment of Mechanical & Aerospace Engineering, Visiting Research Professor at the Southern Illinois University, Edwardsville.

† Professor of Aerospace Engineering, Deptartment of Mechanical & Aerospace Engineering. Associate Fellow AIAA.

Introduction

THE purpose of this study is to develop methods for deriving the stochastic properties of rotor blade vibrations and loads when the blades are subjected to continuous atmospheric turbulence. The difficulty of this task, as compared to the equivalent frozen wing problem, arises mainly from two circumstances. First, a rotor blade in forward flight represents a dynamic system with large periodic variations of damping and stiffness coefficients. Second, the turbulence excitation of the rotor blade represents a nonstationary stochastic process about which no experimental data are presently available. The authors[1] have previously given an introduction to the problem and have developed a perturbation method for computing the time variable mean square flapping response of a rigid rotor blade to an assumed blade angle-of-attack random input, using quasi-steady linearized aerodynamics. The perturbation scheme is valid within a moderate rotor advance ratio range which extends, i.e., at a Lock blade inertia number of 8 to a rotor advance ratio of about 0.6. In this range, reversed flow effects could be neglected and simple analytical functions of azimuth angle could be used for blade damping, blade stiffness, and for the input modulating function. No efforts were made to estimate the actual random input from atmospheric turbulence, since at moderate advance ratio the random shedding of blade trailing vortices are likely to substantially modify in the vicinity of the rotor disk the turbulence characteristics of the free atmosphere.

Although it seems futile to attempt at low rotor advance ratio a stochastic theory without the benefit of experimental data, the case of high rotor advance ratio looks more tractable from the point of view of estimating realistic turbulence inputs. For high rotor advance ratio the flow in the rotor disk is only affected to a minor degree by the vortices shed from the rotor blades. The assumption that each blade feels only the free atmospheric turbulence appears to be plausible and will be made in this paper. Computationally, the treatment of high rotor advance ratios is more complex than the previous analysis. The perturbation scheme must be replaced by a more general method, and reversed flow effects must be included which leads to descriptions of damping, stiffness, and input modulation by nonanalytic functions of time, though quasi-steady linearized aerodynamics are retained. From the practical point of view, the turbulence excited rotor blade vibrations are most significant anyhow in the high rotor advance ratio regime with its well-known high gust sensitivity. Future high-speed rotorcraft may use the high advance ratio regime either for cruising with the main portion of the aircraft weight shifted from the lifting rotor to an auxiliary fixed wing,

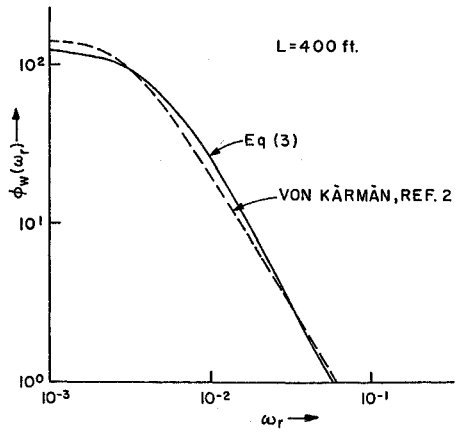

Fig. 1 Power spectral density comparison.

or for transition in flight to or from a stopped and possible stowed lifting rotor condition.

Atmospheric Turbulence

Several analytical descriptions of atmospheric turbulence are in use. The earliest one derived by von Kármán is based on the assumption of isotropic turbulence. The one-sided power spectral density for the vertical turbulence component —the only one to be considered here—is given by the expression,[2]

$$\phi_w(\omega_r) = \sigma_w^2 L[1 + \tfrac{8}{3}(1.34L\omega_r)^2]/[1 + (1.34L\omega_r)^2]^{11/6} \quad (1)$$

where L is the scale length of the longitudinal turbulence component and $L/2$ that of the vertical component. The spectrum is normalized such that

$$\int_0^\infty \phi_w(\omega_r)d\omega_r = \sigma_w^2 \quad (2)$$

The von Kármán spectrum appears to agree better with measured spectra—at least for low altitudes over terrain[3]—than other currently used representations.[4] For altitudes above terrain of 300–700 ft, the scale length was found to be about 400 ft. For high altitudes the scale length is several thousand feet.[5] The standard deviation values of the gust velocity at low altitudes above terrain range from 0 to 9 fps. A standard deviation of 8 fps, which will later be used in numerical examples, occurs with about 0.1% probability. The gust velocity is normal or Gaussian distributed about a zero mean up to 2 standard deviations.[2] Gust velocities of 3 or more standard deviations occur more frequently than in a Gaussian distribution.

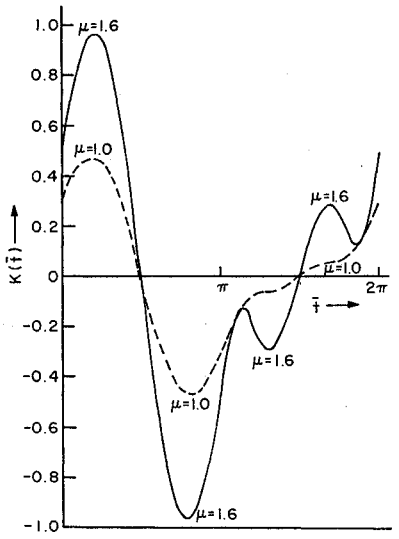

Fig. 2 Aerodynamic blade stiffness parameter.

In this study we will substitute for the power spectral density Eq. (1) with its rather complex autocorrelation function, the following expression:

$$\phi_w(\omega_r) = \sigma_w^2 4L/\pi[4 + (L\omega_r)^2] \quad (3)$$

which corresponds to a simple exponential autocorrelation function,

$$R_w(r) = \sigma_w^2 \exp(-2r/L) \quad (4)$$

The substitute spectrum, Eq. (3), has for small $L\omega_r$ the same constant value $\sigma_w^2 L/\pi$ as the von Kármán spectrum, Eq. (1). A comparison between Eqs. (1) and (3) for $L = 400$ ft in the frequency range of interest here is given in Fig. 1.

The theory to be developed assumes that the rotor blade feels during its entire path the vertical turbulence velocity component as it actually exists only at the rotor center. This means that the vertical turbulence velocity component is assumed to be uniform laterally over the rotor disk,—an assumption often made for the wing span of frozen wing aircraft—and that the random waves encountered by the lifting rotor have wave lengths considerably greater than the rotor radius. The effects of airframe motions and of longitudinal turbulence velocity components on the rotor blades are neglected.

Introducing the flight velocity V and the two-sided power spectrum S_w instead of the one-sided ϕ_w, one obtains for the timewise power spectral density

$$S_w(\omega) = \sigma_w^2 2V/\pi L[(2V/L)^2 + \omega^2] \quad (5)$$

This expression is nondimensionalized by introducing the frequency ratio $\bar{\omega} = \omega/\Omega$ and the velocity ratio $\lambda = w/\Omega R$,

$$S_\lambda(\bar{\omega}) = \sigma^2 a/\pi(a^2 + \bar{\omega}^2) \quad (6)$$

where

$$a = 2\mu/(L/R) \quad (7)$$

and

$$\sigma_\lambda^2 = \int_{-\infty}^{\infty} S_\lambda(\omega)d\omega \quad (8)$$

The timewise autocorrelation function is

$$R_\lambda(\bar{\tau}) = \sigma_\lambda^2 e^{-a|\bar{\tau}|} \quad (9)$$

Blade Flapping at High Advance Ratio

The elastically restrained flapping hinge is assumed for simplicity at the rotor center and the blade is assumed rigid in bending and torsion. Using a frame of reference which rotates with the angular rotor speed Ω, the linearized differential equation of blade flapping has the form

$$\ddot{\beta} + (\gamma/2)C(\bar{t})\dot{\beta} + [P^2 + (\gamma/2)K(\bar{t})]\beta = (\gamma/2)B(\bar{t})\lambda \quad (10)$$

The time unit is $1/\Omega$, the azimuth angle $\Omega t = \bar{t}$. The parameter P has the value one for zero elastic flapping restraint and is larger than one for nonzero restraint, whereby

$$P^2 = 1 + (\omega_\beta/\Omega)^2 \quad (11)$$

The nonanalytic expressions of $C(\bar{t})$, $K(\bar{t})$, and $B(\bar{t})$ taken from Sissingh[6] have been replaced by their respective Fourier series valid over the entire $\bar{t}$ range. Figures 2–4 show these functions at the rotor advance ratios of $\mu = 1.0$ and 1.6, assuming a

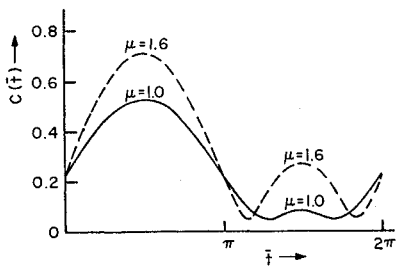

Fig. 3 Aerodynamic blade damping parameter.

tip loss factor of $B = 0.97$. The inflow ratio λ in Eq. (10) is the random input function with zero mean and with the two-sided power spectral density given by Eq. (6). The function $B(\bar{t})$ is called the input modulating function. Figure 5 shows the deterministic solution $y_c(0,\bar{t})$ of Eq. (10) to a unit gust input $\lambda = 1$ for $\mu = 1.6$ and three combinations of parameters which will be retained in the subsequent numerical examples:

$$\left.\begin{matrix} P & 1 & 1.3 & 1.3 \\ \gamma & 4 & 4 & 8 \end{matrix}\right\} \mu = 1.6$$

The analysis has been performed for a step input of $\lambda = 1$ at $\bar{t} = 0$, but in Fig. 5 only, the amost steady-state solution in the third rotor revolution is shown. The computations have been made with a Runge-Kutta method,[7] which for a step size of h has a truncation error of the order of $0(h^5)$, whereby a step size of $h = 0.2$ has been selected for $\Delta\bar{t}$.

Figure 5 shows that at constant γ the maximum flapping deflection decreases with increasing P because of the added elastic flapping restraint, and that at constant P the maximum flapping deflection increases with increasing γ because of the lower centrifugal moment restraint in relation to the aerodynamic moments.

It is of interest to know the flapping stability margins for these three cases. According to Floquet's theory, the solution of the left-hand side of Eq. (10) can be written for $\eta_1 \neq \eta_2$ in the form[8]

$$\begin{Bmatrix} \beta(\bar{t}) \\ \dot{\beta}(\bar{t}) \end{Bmatrix} = [A(\bar{t})] \begin{Bmatrix} \alpha_1 \exp(\eta_1 \bar{t}) \\ \alpha_2 \exp(\eta_2 \bar{t}) \end{Bmatrix} \tag{12}$$

$[A(\bar{t})]$ is a 2×2 matrix of time functions periodic with 2π; α_1, α_2 are time constants derived from the initial conditions. The motion is stable if the real parts $Re(\eta_1)$, $Re(\eta_2)$ are negative and the stability margin can be defined by the smallest value of $|Re(\eta)|_{\min}$. These minimum values for the 3 cases have been computed by D. A. Peters with the help of the Floquet transition matrix[9]:

$$\left.\begin{matrix} P & 1 & 1.3 & 1.3 \\ \gamma & 4 & 4 & 8 \\ |\mathrm{Re}(\eta)|_{\min} & 0.22 & 0.34 & 0.27 \end{matrix}\right\} \mu = 1.6$$

Adding elastic restraint—increasing P from 1 to 1.3—increases the stability margin. Reducing the centrifugal restraint in relation to the aerodynamic moments— increasing γ from 4 to 8—reduces the stability margin.

Stochastic Response Analysis

We first assume that a Fourier transform of the time function $\lambda(\bar{t})$ in Eq. (10) exists. Writing this Fourier transform $\Lambda(f)$, with $f = \omega/2\pi$, the inverse Fourier transform is

$$\lambda(\bar{t}) = \int_{-\infty}^{\infty} \Lambda(f) e^{i2\pi f\bar{t}} df \tag{13}$$

Since the time function $B(\bar{t})$ can be shifted to the right of the frequency integral, the right-hand side of Eq. (10) reads

$$0.5\gamma B(\bar{t})\lambda(\bar{t}) = 0.5 \int_{-\infty}^{\infty} \Lambda(f)\gamma B(\bar{t}) e^{i2\pi f\bar{t}} df \tag{14}$$

Because of the linearity of Eq. (10), the particular solution $\beta(\bar{t})$ can now be written in the form

$$\beta(\bar{t}) = \int_{-\infty}^{\infty} \Lambda(f) y_B(f,\bar{t}) df \tag{15}$$

where $y_B(f,\bar{t})$ is the complex valued response to the input $0.5\gamma B(t)e^{i2\pi ft}$ with zero initial conditions. Differentiating Eq. (15) with respect to time, one obtains

$$\dot{\beta}(\bar{t}) = \int_{-\infty}^{\infty} \Lambda(f) \dot{y}_B(f,\bar{t}) df \tag{16}$$

In general, $\lambda(\bar{t})$ is a nonstationary random process with the double frequency power spectral density

$$S_{\lambda\lambda}(f_1,f_2) = E[\Lambda^*(f_1)\Lambda(f_2)] \tag{17}$$

The response autocorrelation function is then given by

$$R_{\beta\beta}(\bar{t}_1,\bar{t}_2) = E[\beta^*(\bar{t}_1)\beta(\bar{t}_2)] = \iint_{-\infty}^{\infty} S_{\lambda\lambda}(f_1,f_2) y_B^*(f_1,\bar{t}_1) y_B(f,\bar{t}) df_1 df_2 \tag{18}$$

Assuming now, as mentioned before, that the blades feel at any instant the vertical velocity $\lambda(\bar{t})$ existing at the rotor center and further assuming uniform turbulence characteristics in the atmosphere and uniform flight speed, the time function $\lambda(\bar{t})$ represents a stationary stochastic process for which

$$S_{\lambda\lambda}(f_1,f_2) = S_\lambda(f_1)\delta(f_2 - f_1) \tag{19}$$

where $\delta(f)$ is the Dirac delta function. Inserting Eq. (19) into Eq. (18), one obtains

$$R_{\beta\beta}(\bar{t}_1,\bar{t}_2) = \int_{-\infty}^{\infty} S_\lambda(f) y_B^*(f,\bar{t}_1) y_B(f,\bar{t}_2) df \tag{20}$$

With $S_\lambda(f) = 2\pi S_\lambda(\omega)$, Eq. (20) can also be written in the form

$$R_{\beta\beta}(\bar{t}_1,\bar{t}_2) = \int_{-\infty}^{\infty} S_\lambda(\omega) y_B^*(\omega,\bar{t}_1) y_B(\omega,\bar{t}_2) d\omega \tag{21}$$

Setting $\bar{t}_1 = \bar{t}_2$, one obtains the time variable variance

$$\sigma_\beta^2(\bar{t}) = R_{\beta\beta}(\bar{t},\bar{t}) = \int_{-\infty}^{\infty} S_\lambda(\omega) y_B^*(\omega,\bar{t}) t_B(\omega,\bar{t}) d\omega \tag{22}$$

For numerical computations it is preferable to introduce the responses $y_c(\omega,\bar{t})$, $y_s(\omega,\bar{t})$ to the inputs $0.5\gamma B(t)\cos(\omega,\bar{t})$, and $0.5\gamma B(t)\sin(\omega,\bar{t})$, respectively. Eq. (22) then assumes the form

$$\sigma_\beta^2(\bar{t}) = 2\int_0^{\infty} \{y_c^2(\omega,\bar{t}) + y_s^2(\omega,\bar{t})\} S_\lambda(\omega) d\omega \tag{23}$$

Using Eqs. (15) and (16) and determining the autocorrelation function for the response rate,

$$R_{\dot{\beta}\dot{\beta}}(\bar{t}_1,\bar{t}_2) = E[\dot{\beta}^*(\bar{t}_1)\dot{\beta}(\bar{t}_2)] \tag{24}$$

and the cross correlation function

$$R_{\beta\dot{\beta}}(\bar{t}_1,\bar{t}_2) = E[\beta^*(\bar{t}_1)\dot{\beta}(\bar{t}_2)] \tag{25}$$

one obtains with the same assumptions as before the time

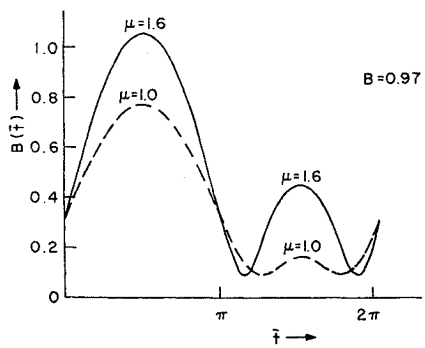

Fig. 4 Input modulating function.

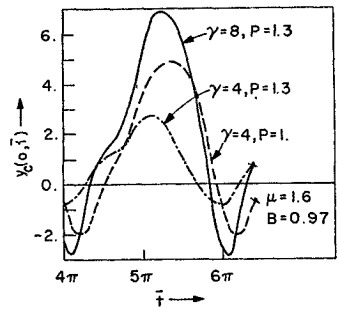

Fig. 5 Deterministic blade responses.

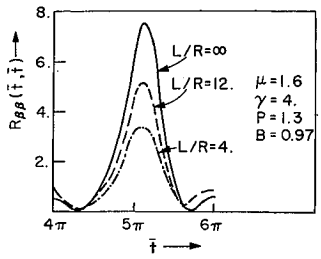

Fig. 6 Effect of L/R on the mean square response.

variable variance of the response rate

$$\sigma_{\dot\beta}^2(\bar t) = 2\int_0^\infty \{\dot y_c^2(\omega,\bar t) + \dot y_s^2(\omega,\bar t)\}S_\lambda(\omega)d\omega \qquad (26)$$

and the time variable cross correlation between the response and the response rate,

$$r(\bar t)\sigma_\beta(\bar t)\sigma_{\dot\beta}(\bar t) = 2\int_0^\infty \{y_c(\omega,\bar t)\dot y_c(\omega,\bar t) + y_s(\omega,t)\dot y_s(\omega,\bar t)\}S_\lambda(\omega)d\omega \qquad (27)$$

The cross correlation coefficient $r(\bar t)$ can have only values between -1 and $+1$. If we now stipulate that the turbulence velocity components represent a Gaussian random process with zero mean, then the response and the rate of change of the response are also Gaussian with zero mean. This conclusion follows from the linearity of Eq. (10).

Of particular importance for the design of fatigue tests or the estimate of fatigue allowables is the expected value of the number of upward crossings per unit time N of a threshold ζ of the response variable β: $E[N_+(\zeta,\bar t)]$. Knowing this function, it is possible under certain conditions to estimate approximately the distribution of the higher level peaks which determines the fatigue damage to a structure.[10,11] If $P_{\beta\dot\beta}(\beta,\dot\beta,\bar t)$ is the time variable joint probability of obtaining at the time $\bar t$, the response β, and the rate of response $\dot\beta$, the threshold crossing expectation is given by

$$E[N_+(\zeta,\bar t)] = \int_0^\infty \dot\beta P_{\beta\dot\beta}(\zeta,\dot\beta,\bar t)d\dot\beta \qquad (28)$$

where the joint probability is[11,12]

$$P_{\beta\dot\beta}(\beta,\dot\beta,\bar t) = [1/2\pi\sigma_\beta\sigma_{\dot\beta}(1-r^2)^{1/2}]\exp\{-[\sigma_\beta^2\dot\beta^2 - 2\sigma_\beta\sigma_{\dot\beta}r_{\beta\dot\beta} + \sigma_{\dot\beta}^2\beta^2]/2\sigma_\beta^2\sigma_{\dot\beta}^2(1-r^2)^{1/2}\} \qquad (29)$$

Inserting Eq. (29) for $\beta = \zeta$ into Eq. (28) and performing the integrations over $d\dot\beta$, one obtains

$$E[N_+(\zeta,\bar t)] = (\tfrac{1}{2}\pi)(1-r^2)^{1/2}(\sigma_{\dot\beta}/\sigma_\beta)\exp\{-(\zeta/\sigma_\beta)^2/2(1-r^2)\} + \{\tfrac{1}{2}(2\pi)^{1/2}\}(\sigma_{\dot\beta}/\sigma_\beta)(\zeta r/\sigma_\beta)\{\exp[-(\zeta^2/2\sigma_\beta^2)]\}\times(1+\mathrm{erf}\{\zeta r/\sigma_\beta[2(1-r^2)]^{1/2}\}) \qquad (30)$$

where

$$\mathrm{erf}(x) = [2/(\pi)^{1/2}]\int_0^x e^{-\theta^2}d\theta$$

The quantities σ_β, $\sigma_{\dot\beta}$, r are time functions to be computed from Eqs. (23), (26), and (27), respectively.

For a stationary Gaussian process we have $r = 0$, and Eq. (30) reduces to the well-known positive threshold crossing equation,

$$E[N_+(\zeta)] = (\tfrac{1}{2}\pi)(\sigma_{\dot\beta}/\sigma_\beta)\exp[-(\zeta/\sigma_\beta)^2/2] \qquad (31)$$

For $\zeta = 0$ one obtains from Eq. (30) the expected number of positive zero crossings per unit time:

$$E[N_+(0,\bar t)] = (\tfrac{1}{2}\pi)(1-r^2)^{1/2}\sigma_{\dot\beta}/\sigma_\beta \qquad (32)$$

For a stationary Gaussian process we have $r = 0$, and Eq. (32) reduces to the well-known expression

$$E[N_+(0)] = (\tfrac{1}{2}\pi)\sigma_{\dot\beta}/\sigma_\beta = (\tfrac{1}{2}\pi)\left[\int_{-\infty}^\infty \omega^2 S_\beta(\omega)d\omega \Big/ \int_{-\infty}^\infty S_\beta(\omega)d\omega\right]^{1/2} \qquad (33)$$

Numerical Results

The same three examples for which Fig. 5 shows the deterministic response to a unit input of λ have been used to compute $\sigma_\beta^2(\bar t)$, $\sigma_{\dot\beta}^2(\bar t)$, $r(\bar t)$, and $E[N_+(\zeta,\bar t)]$ from Eqs. (23, 26, 27, and 30), respectively. The deterministic responses $y_c(\omega,\bar t)$ and $y_s(\omega,\bar t)$ were computed with a Runge-Kutta method,[7] with a truncation error of order $0(h^5)$, and stepsize $h = \Delta\bar t = 0.2$. The nonanalytic periodic functions $K(\bar t)$, $C(\bar t)$, and $B(\bar t)$ shown in Figs. 2–4 were replaced by their 16-term Fourier series. The input power spectral density $S_\lambda(\bar\omega)$ was assumed according to Eqs. (6) and (7) with $\sigma_\lambda^2 = 1$, $\mu = 1.6$, and two L/R values = 12 and 4. Large savings in computer time have been achieved by using a canonical expansion for $S_\lambda(\bar\omega)$. A sample function $\lambda(t)$, belonging to a stationary random process with zero mean, can be approximated to any desired accuracy (in the mean square sense) by a canonical expansion of the form[13]

$$\lambda(t) = \sum_{\nu=-N}^{N} V_\nu e^{i\omega_\nu t} \qquad (34)$$

where the uncorrelated random coefficients V_ν have zero mean values and variances given by

$$E[|V_\nu|^2] = \int_{\omega_\nu-\alpha}^{\omega_\nu+\alpha} S_\lambda(\omega)d\omega, \quad \nu = 0,\pm1,\ldots\pm N \qquad (35)$$

the autocorrelation function is

$$R_\lambda(t_2-t_1) = E[\lambda^*(t_1)\lambda(t_2)] = \sum_{\nu=-N}^{N} E[|V_\nu|^2]e^{i\omega_\nu(t_2-t_1)} \qquad (36)$$

The Fourier transform of Eq. (36) then results in

$$S_\lambda(\omega) = \sum_{\nu=-N}^{N} E[|V_\nu|^2]\delta(\omega-\omega_\nu) \qquad (37)$$

whereby the weighting factors for the delta functions are given by Eq. (35). A canonical expansion of $S_\lambda(\omega)$ then is obtained by dividing the positive frequency range into N intervals, selecting inside each interval a central frequency ω_ν and multiplying $\delta(\omega-\omega_\nu)$ with the integral of $S_\lambda(\omega)$ over this interval.

Using a canonical representation Eq. (37) of $S_\lambda(\omega)$ with $N = 11$ and a Runge-Kutta routine with $\Delta\bar t = 0.2$ stepsize for the $y_s(\omega,\bar t)$ and $y_s(\omega,\bar t)$, functions the computations of Eqs. (23, 26, 27) and the evaluation of Eq. (30) for seven thresholds over a time range of $\bar t = 0$ to 20 required for a given condition about 3 min. of IBM 360/50 machine time.

Figure 6 shows the effect of the ratio of turbulence scale length over rotor radius L/R on the mean square response $\sigma_\beta^2(\bar t) = R_{\beta\beta}(\bar t,\bar t)$ for $\mu = 1.6$, $\gamma = 4$, and $P = 1.3$. As in Fig. 5, only the third rotor revolution is shown where the mean square response has become periodic with period 2π. Low altitude turbulence scale lengths L typical for rotorcraft operation are in the order of 400 ft[3]. For a small rotorcraft with 16-ft rotor radius, we then have $L/R = 25$, for a medium rotorcraft with 33-ft rotor radius, we have $L/R = 12$ and for a very large rotorcraft with a rotor radius of 100 ft (not as yet in existence), we would have $L/R = 4.0$. Figure 6 brackets, therefore, actual conditions in low-level flight, and indicates

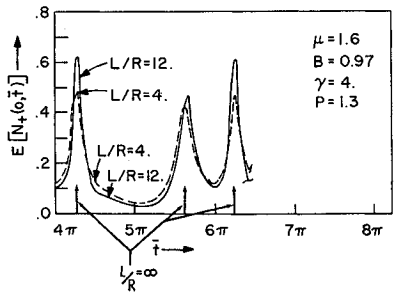

Fig. 7 Effect of L/R on positive zero crossing expectation.

that the turbulence response of rotor blades decreases with increasing rotor size.

For high-altitude flight with a turbulence scale length L of several thousand feet, the assumption $L/R = \infty$ is a good approximation and leads to a very simple "quasi deterministic" analysis. We then have $a = 0$ in Eqs. (6) and (9), which result in

$$R_\lambda(\bar{\tau}) = \sigma_\lambda^2 \quad S_\lambda(\bar{\omega}) = \sigma_\lambda^2 \delta(\bar{\omega}) \tag{38}$$

where $\delta(\bar{\omega})$ is the Dirace delta function. Inserting Eq. (38) into Eq. (23) one obtains

$$\sigma_\beta^2(\bar{t}) = y_c^2(0,\bar{t}) \int_{-\infty}^{\infty} S_\lambda(\omega) d\omega = y_c^2(0,\bar{t}) \sigma_\lambda^2 \tag{39}$$

The function $y_c(0,\bar{t})$ is the deterministic response to the input $0.5\gamma B(\bar{t})$ shown in Fig. 5. Equation (39) states that for the "quasi deterministic" case $L/R = \infty$, that is when the rotor radius is small as compared to the turbulence scale length, the response variance $\sigma_\beta^2(\bar{t})$ is equal to the squared deterministic response for $\lambda = 1$ multiplied by the variance of the inflow process (assumed to be one in all figures). If the input is Gaussian with zero mean, then the response for each value of time $\bar{t}$ is also Gaussian with zero mean.

Figure 7 shows for the same example and for the two L/R values 4 and 12 the time variable expected number of positive zero crossings per unit time, as computed from Eq. (32). For $L/R = \infty$ the zero crossings are concentrated at the two locations per period indicated in Fig. 7, which is consistent with the zero crossing pattern shown in Fig. 5. One should note that positive and negative vertical turbulence velocities occur on the average with equal frequency so that during some rotor revolutions the response for $L/R = \infty$ will look like a curve in Fig. 5, for an equal number of revolutions the response will be given by the mirror image of this curve. On the average, in two rotor revolutions a positive zero crossing will occur once in the first quadrant followed by a similar crossing in the fourth quadrant. For finite values of L/R, Fig. 7 shows that zero crossings can occur at any time, with the most likely occurrences close to those for $L/R = \infty$. The area under the curves in Fig. 7 between 4π and 6π represents the expected number of positive zero crossings per revolution. Integrating the curves between 4π and 6π, one obtains a value close to one, same as for $L/R = \infty$.

The fact evident from Fig. 7 that most of the zero crossings occur within narrow ranges of azimuth angle can also be expressed by stating that the phase angles of the random flapping oscillations have certain sharp peaks in their distribution. If one considers only the first harmonic in the flapping response with period 2π which, according to Fig. 5 is dominant, one can say that blade flapping from atmospheric turbulence represents a quasi-coherent narrow-band random process with small phase angle variance. Measured sample functions of blade flapping in a wind tunnel where artificial turbulence was induced by a lattice of 1-in. square bars spaced at one foot centers and covering a 9 ft × 4 ft area confirm this character quite clearly.[14]

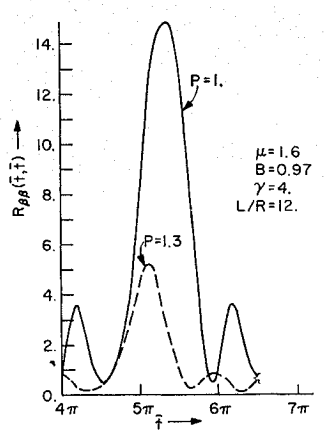

Fig. 8 Effect of P on the mean square response.

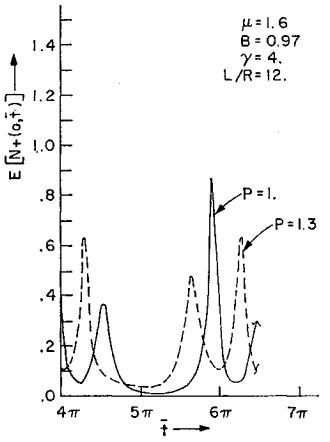

Fig. 9 Effect of P on positive zero crossing expectation.

Figure 8 shows the effect of elastic blade root restraint on the mean square response, assuming $\gamma = 4$ and $L/R = 12$. The elastically restrained blade with $P = 1.3$ shows a large reduction in response as compared to the freely flapping blade. In order to obtain dimensional values, one can assume a standard deviation for the vertical turbulence velocity $\sigma_w = 8$ fps, which at low altitude occurs with 0.1% probability.[3] Assuming $\Omega R = 300$ fps for an unloaded rotor crusing with $\mu = 1.6$ at 280 knots, one obtains $\sigma_\lambda = 8.57.3/300 = 1.5°$. The maximum flapping response standard deviation, according to Fig. 8, is then 5.8° for $P = 1$ and 3.4° for $P = 1.3$. Since three standard deviations occur in a Gaussian distribution with 0.002% probability, in the actual distribution about 10 times more frequent,[2] very large random flapping angles can occasionally be encountered. These flapping angles can also be expressed in terms of "load factors," based on a one g hovering load. If $\bar{\alpha}$ is the mean blade angle of attack in hovering, the coning angle is approximately $\bar{\alpha}\gamma/8P^2$. Using $\bar{\alpha} = 6°$ and $\gamma = 4$ as in Fig. 8, one obtains for $P = 1$ and 1.3 coning angles of 3° and 1.8°, respectively. The flapping angle from a vertical turbulence velocity with 8 fps standard deviation then produces a "load factor" with a standard deviation of almost ±2.0, and "load factors" of ±4.0 and higher will occasionally occur. This may be unacceptable either from a point of view of blade-fuselage interference or from a stress point of view.

Figure 9 shows for $L/R = 12$ the effect of elastic root restraint on the expected number of positive zero crossings per unit time. Again the maxima occur approximately at the corresponding zero crossings of the $y_c(0,\bar{t})$ curves shown in Fig. 5, and the average number of positive zero crossings per revolution is about one. Figures 10 and 11 show for $L/R = 12$ the

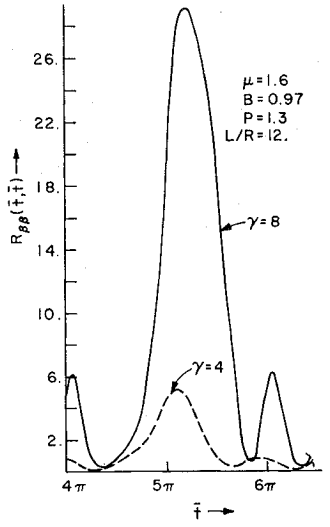

Fig. 10 Effect of γ on mean square response.

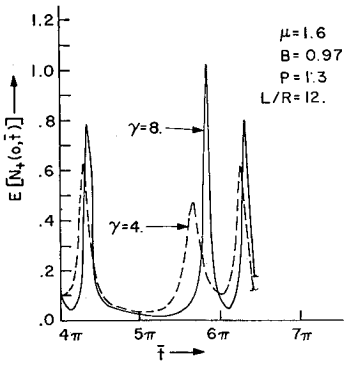

Fig. 11 Effect of γ on positive zero crossing expectation.

effect of Lock inertia number on the mean square response and on the expected number of positive zero crossings per unit time. The lighter blade ($\gamma = 8$) exhibits much larger flapping angles.

Figure 12 shows for $\gamma = 4$, $P = 1.3$, $L/R = 12$ the expected number of positive threshold crossings per unit time for the thresholds 1.75, 2.5, 3.0, and 4.0. It is seen that one of the bell shaped distributions disappears with increasing threshold level and that only the primary bell shaped distribution remains. It is centered at about the forward blade position. By integrating the area for this distribution and plotting it vs the threshold, one obtains Fig. 13, which gives for the high response levels the expected number of positive threshold crossings per revolution. Because of the small variance of the response phase indicated in Fig. 12, one can interpret Fig. 13 also as giving approximately the expected number of positive response peaks per revolution above the threshold ζ. The number of negative response peaks will be the same. Figure 13 can thus be used to evaluate turbulence related fatigue loads. For $L/R = \infty$ the expected number of response peaks per revolution above a level ζ can be easily determined from the Gaussian distribution with the standard deviation given by Eq. (39).

Conclusion

The main assumptions of the analysis are 1) rigid blades attached to a fixed hub with central elastically restrained flapping hinges; 2) quasi-steady linearized aerodynamics including reversed flow effects; and 3) inflow uniform over the rotor disk with random time variations representing a stationary Gaussian process. Under these assumptions, the time variable blade flapping response variance and the threshold crossing expectations can be computed with relatively little computational effort. The flapping response to typical atmospheric turbulence conditions is a quasi-coherent narrow-band random process. The threshold crossing characteristics allow a simple estimation of high level response peak distributions

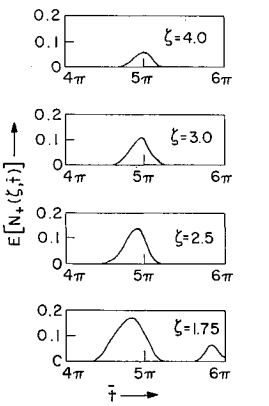

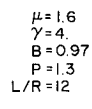

Fig. 12 Expected positive threshold crossings per unit time.

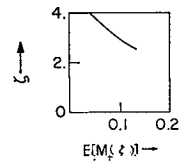

Fig. 13 Expected positive threshold crossings per revolution.

needed for fatigue considerations. Based on low-altitude atmospheric turbulence characteristics, high random flapping angles or root bending moments can occur at an advance ratio of 1.6 and 280 knots flight speed, representative of a slowed unloaded rotor, indicating the necessity of gust alleviating means for such a rotor.

Topics for continued studies of random blade vibrations and loads are 1) relaxation of the assumption of spacewise uniform inflow to obtain the effects of spatial distribution of turbulence in the rotor disk; 2) effects of gust alleviating methods; 3) development of experimental methods of evaluating random blade vibrations and loads; 4) development of a rotor disk turbulence model with parameters to be determined from the measured random blade response; 5) development of a multiblade analysis including the random airframe motion; and 6) development of an elastic blade random response analysis.

Inspite of these many gaps, the theory developed so far appears to be adequate within the stated limitations to estimate the principal effects of atmospheric turbulence on unloaded rotors operating at high advance ratio.

References

[1] Gaonkar, G. H. and Hohenemser, K. H., "Flapping Response of Lifting Rotor Blades to Atmospheric Turbulence," *Journal of Aircraft*, Vol. 6, No. 6, Nov.-Dec. 1969, pp. 496–503.

[2] Houbolt, J. C., Steiner, R., and Pratt, K. G., "Dynamic Response of Airplanes to Atmospheric Turbulence including Flight Data on Input and Response," TR R-199, 1964, NASA.

[3] Gault, J. D. and Gunter, D. E., "Atmospheric Turbulence Considerations for Future Aircraft Designed to Operate at Low Altitudes," *Journal of Aircraft*, Vol. 5, No. 6, Nov.-Dec. 1968, pp. 574–577.

[4] Burns, A., "Power Spectra of Low Altitude Atmospheric Turbulence measured from an Aircraft," Technical Note Structures 329, 1963, Royal Aircraft Establishment, England.

[5] Steiner, R. and Pratt, K. G., "Some Applications of Power Spectra to Airplane Turbulence Problems," *Journal of Aircraft*, Vol. 4, No. 4, July-Aug. 1967, pp. 360–365.

[6] Sissingh, G. J., "Dynamics of Rotors Operating at High Advance Ratios," *Journal of American Helicopter Society*, Vol. 13, No. 3, July 1968, pp. 56–63.

[7] Hildebrand, F. B., *Introduction to Numerical Analysis*, McGraw-Hill, New York, 1956, pp. 236–238.

[8] Kaplan, W., *Operational Methods of Linear Systems*, Addison Wesley, Reading, Mass., 1962, pp. 472–488.

[9] Peters, D. A. and Hohenemser, K. H., "Application of the Floquet Transition Matrix to Problems of Lifting Rotor Stability," Paper 412, June 1970, 26th National Forum of the American Helicopter Society, Washington, D.C.

[10] Shinozuka, M. and Yang, J. N., "Nonstationary Peak Distribution," *Probablistic Concepts and Methods in Engineering, Proceedings of the ASCE-EMD Specialty Conference*, Purdue, Nov. 1969, pp. 169–173.

[11] Lin, Y. K., *Probablistic Theory of Structural Dynamics*, McGraw-Hill, New York, 1967, pp. 296–309.

[12] Leadbetter, M. R. and Cryer, J. D., "On the Mean Number of Curve Crossings by Non-Stationary Normal Processes," *Annals of Mathematical Statistics*, Vol. 36, 1965, pp. 509–516.

[13] Pugachev, V. S., *Theory of Random Functions and its Application to Control Problems*, Pergamon Press, New York, 1965, pp. 324–326.

[14] Grant, B. E., "A Method for Measuring Aerodynamic Damping of Helicopter Rotors in Forward Flight," *Journal of Sound and Vibration*, Vol. 3, 1966, pp. 407–421.